International Journal of Heat and Mass Transfer 52 (2009) 133–141

Contents lists available at ScienceDirect

International Journal of Heat and Mass Transfer

journal homepage: www.elsevier.com/locate/ijhmt

Analytical solution for solidification of close-celled metal foams

B. Zhang [a], T. Kim [b], T.J. Lu [b,c,*]

[a] State Key Laboratory for Mechanical Behavior of Materials, Xi'an Jiaotong University, Xi'an, 710049, PR China
[b] MOE Key Laboratory for Strength and Vibration, Xi'an Jiaotong University, Xi'an 710049, PR China
[c] Department of Engineering, University of Cambridge, Cambridge CB2 1PZ, UK

ARTICLE INFO

Article history:
Received 18 February 2008
Received in revised form 2 June 2008
Available online 25 July 2008

Keywords:
Effective thermal conductivity
Metal foam
Numerical simulation
Porosity
Solidification

ABSTRACT

This paper introduces an analytical model capable of predicting the location of solidification front as well as the full solidification time for heterogeneous materials such as close-celled metallic foams. Full numerical simulations with the method of finite difference are separately conducted to validate the analytical model. The model predicts that an increase in porosity causes significant retardation of full solidification as a result of decreased effective thermal conductivity and diffusivity of the porous medium. Effects of pore shape and cooling temperature on overall solidification behavior were also studied.

1. Introduction

Phase change occurring with solidification (or melting), generally known as the "Stefan problems", is associated with many practical applications such as castings, welding, heat treatment, thermal energy storage, and freezing or thawing of soils and foods [1–3]. Such problems were pioneered by Stefan [4] who first examined the transfer of heat during the phase change of icecap in the North Pole. Due to mathematical complexities in Stefan problems, only a few exact solutions are at present available including Neumann's solutions for the solidification of a semi-infinite slab melt. In Neumann's solution, the temperature of the slab melt is taken as temporally and spatially invariant and, for cooling, a sudden introduction of a constant temperature is imposed at the wall boundary.

Despite the importance of Stefan or Stefan-type problems and the continuous efforts made by numerous studies, analytical solutions of such phase change problems are still limited to a few idealized situations. This is mainly because of the moving boundaries (interfaces) among different phases, the locations of which are essentially unknown. A comprehensive review of existing exact solutions can be found in Carslaw and Jaeger [5]. On the other hand, numerous approximate methods including heat balance integral [6], moving heat source [7], and perturbation [8] have been proposed to simplify the problem.

Previous efforts for examining how a phase interface evolves in time mainly deal with the solidification or melting process in "homogeneous" (dense) materials. However, no "pure" homogeneous materials exist as all engineering materials contain more than one phase and hence are, exactly speaking, "heterogeneous" materials. One of the emerging heterogeneous materials is metallic foams having either closed or open cells. The low densities and novel physical, mechanical, thermal, electrical, and acoustic properties of the metal foams have led to a diverse range of practical applications such as ultra-lightweight structures, energy absorption, thermal management, and sound absorption [9].

A typical fabrication route of close-celled aluminum foams is direct foaming, as illustrated in Fig. 1. In this technique [10], calcium is firstly added to aluminum melt at 680 °C. The melt is then stirred for several minutes whilst its viscosity continuously increases due to the formation of calcium oxide (CaO). After the viscosity of the melt has reached a desirable value, TiH_2 which serves as the blowing agent by releasing hydrogen is added to the melt. The melt soon starts to expand slowly and gradually fills the foaming vessel. As the vessel is cooled below the melting temperature of the mixture, the melt foam turns into solid state.

2. Processing of close-celled metallic foams: control of pore morphologies

Traditionally, close-celled aluminum foams with polygonal pores and porosities higher than 0.8 (Zone I) have been developed [11–15], as shown in Fig. 2. With recent advances in processing technologies, aluminum foams with high porosities and small polygonal pores (Zone II) [16] or low porosities and spherical pores

* Corresponding author. Address: MOE Key Laboratory for Strength and Vibration, Xi'an Jiaotong University, Xi'an 710049, PR China. Tel.:+86 29 82665600; fax: +86 29 83234781.
E-mail address: tjlu@mail.xjtu.edu.cn (T.J. Lu).

0017-9310/$ - see front matter © 2008 Elsevier Ltd. All rights reserved.
doi:10.1016/j.ijheatmasstransfer.2008.06.006

Nomenclature

c_p	specific heat of solid materials [J/(kg K)]
f_s	solid fraction
H	total thickness of melt along the direction of solidification [m]
$\widetilde{H}$	enthalpy [J]
$\tilde{h}$	sensible enthalpy [J]
k_e	effective thermal conductivity of porous materials [W/(m K)]
k_s	thermal conductivity of dense solid materials [W/(m K)]
L	latent heat [J/Kg]
q''	heat flux though solidified layer [W/m^2]
S	thickness of solidification layer [m]
t	time [s]
T_0	cooling temperature [K]
$T_{liquidus}$	liquidus temperature [K]
$T_{solidus}$	solidus temperature [K]
T_m	melting temperature [K]
T_s, T_l	solid and melt temperature [K]
x	coordinate coinciding with solidification

Greek symbols

α_e	effective thermal diffusivity of porous materials [m^2/s]
α_s	thermal diffusivity of dense solid materials [m^2/s]
β	shape factor
ε	porosity
χ	non-dimensional position (=x/H)
θ	non-dimensional temperature (=$(T-T_0)/(T_m-T_0)$)
λ	constant defined by Eq. (7)
ξ	non-dimensional solidification front (=S/H)
ρ_e	effective density of porous materials [kg/m^3]
ρ_s	density of solid composition [kg/m^3]
τ	non-dimensional time (=$\alpha_s t/H^2$)

Subscripts

e	effective value
l	liquid phase
ref	reference value
s	solid phase
0	at $x = 0$
H	at $x = H$

(Zone III and Zone IV) [17,18] have been manufactured. Therefore, for closed-celled aluminum foams, the pore shape can be categorized into three groups according to the porosity (denoted here as ε): spherical pores, sphere-like pores, and polygonal pores. For most close-celled aluminum foams with relatively low porosity ($\varepsilon < 0.7$), the pores are likely to be spherical; as the porosity is increased beyond 0.8, the pores tend to become polygonal; the pores will be sphere-like when the porosity lies between 0.7 and 0.8 [15]. It can be concluded from Fig. 2 that if the pore size and porosity of close-celled aluminum foam are fixed, its pore shape is also fixed.

It has been established that close-celled metallic foams with different pore morphologies also exhibit different load-bearing and energy-absorbing properties [17,18]. For instance, experimentally, it was found that close-celled Al alloy foams with spherical pores have superior energy absorption properties in comparison with foams having polygonal pores; (see Fig. 3) [18]. For the same uniaxial compressive strain level of 0.5, the deformation energy of Al alloy foams with spherical pores ($\varepsilon = 0.673$) is 2.6 times that of Al alloy foams with polygonal pores ($\varepsilon = 0.886$). How to manufacture close-celled metallic foams with desirable pores shapes via the foaming route has therefore become an important issue for a variety of engineering applications such as transportation and aerospace engineering.

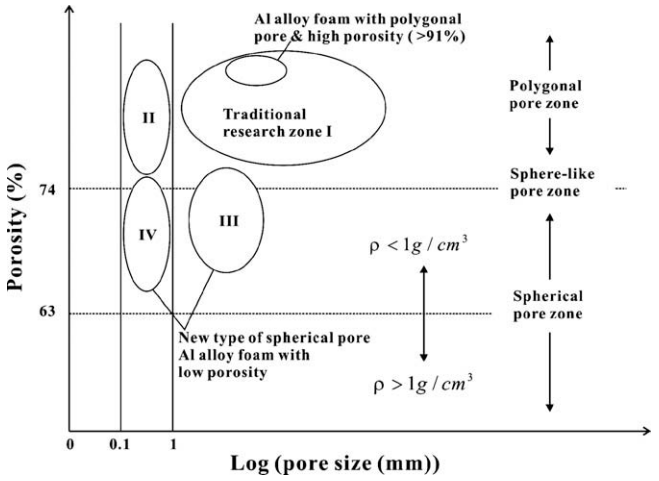

Fig. 2. Cross-relationship amongst porosity, pore size and pore shape for close-celled aluminum foams [15];

Porosity, pore size and pore shape are the three main factors controlling the cellular morphology of a close-celled metallic foam.

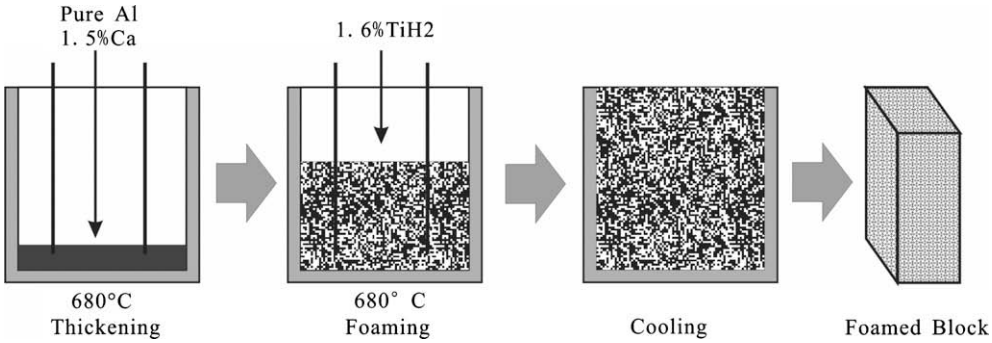

Fig. 1. Process route of direct foaming method for metal melts ("Alporas – process") [10].

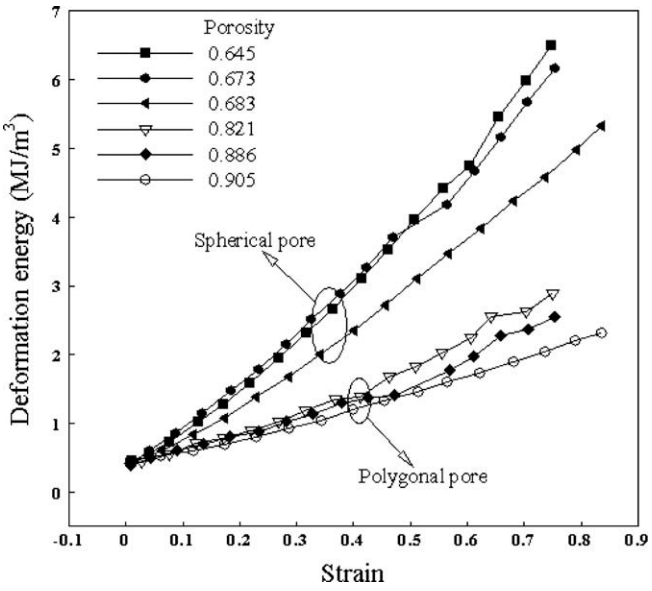

Fig. 3. Effect of pore shape (porosity) on energy absorption capability of close-celled aluminum foams [18].

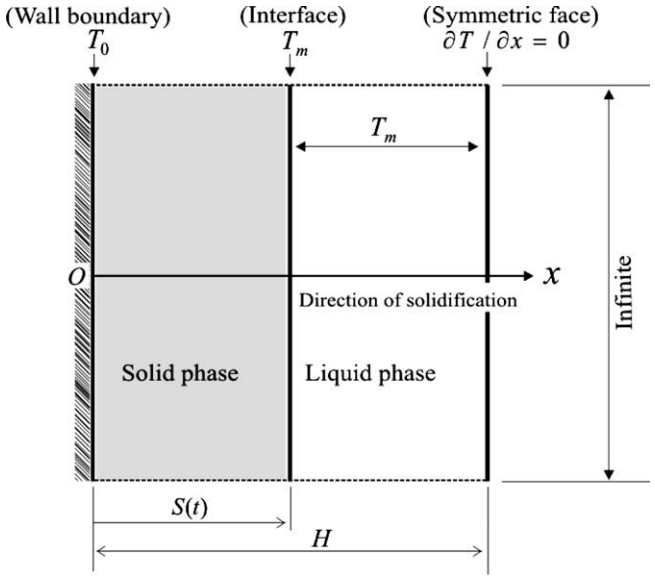

Fig. 4. Geometry and boundary conditions for one-dimensional Stefan problem in a finite region.

To process metallic foams with a tighter control of pore morphologies requires establishing the inherent relationships amongst pore size, porosity and pore shape, as well as the general framework of processing steps and techniques affecting pore structure control during foaming. To this end, a better understanding of the complicated foaming and solidification process becomes a key step. It has been demonstrated that the evolution of cellular structure is influenced by many processing factors such as the viscosity, foaming time and solidification mode [15,19,20]. This makes the foaming and solidification processes extremely complicated, leading to difficulties in pore structure control.

To obtain pure aluminum foams having high porosity, it needs not only to precisely control the porosity by using the relationship between porosity and foaming time, but also to solidify the melt in time during the plateau stage on the porosity–time curve to control the pore size and uniformity of pore distribution [15]. To obtain aluminum alloy foams, in addition to the steps mentioned above, multi-directional solidification is also needed in order to overcome the shrinkage caused by the *additional force field* during cooling [21]. For high strength aluminum alloy foams having spherical pores and relatively low porosities, a suitable amount of vesicant (about 1.0%) and proper stirring time (about 100 s) are required in order to drop the plateau stage of porosity-time curve to the low porosity regime [15].

The focus of this study is to analytically examine how the solidification front (interface between two phases) proceeds in time under various cooling conditions. The present analysis is limited to close-celled metal foams consisting of dense materials and randomly spaced gaseous pores, with aluminum foam chosen as the prototype. In the proposed analytical model, an existing model for the effective thermal conductivity of porous media as a function of both the porosity and pore shape is coupled with one of the classical solutions (Neumann's solution) to account for the influence of pores in the solidification process. Full numerical simulations with the method of finite difference are separately conducted to validate the predictions of the analytical model.

3. One-dimensional Stefan problem for dense materials

An analytical solution is available for a classical but fundamental solidification problem described as: one side of the melt with total thickness of H, initially at melting temperature T_m, is suddenly exposed to temperature T_0 ($T_0 < T_m$) at time $t > 0$, so that the solidification takes place from $x = 0$ as illustrated in Fig. 4. For simplicity, the melt is assumed to be infinitely wide, indicating one-dimensional problem along the x-axis. When the wall temperature at $x = 0$ begins to drop below T_m, a portion of the internal heat is liberated triggering the onset of solidification. All of the relevant physical properties of the material (in either liquid or solid state) such as the latent heat (L), thermal conductivity (k_s), diffusivity (α_s), and specific heat at constant pressure (c_p) are further assumed to be invariant in temperature, time, and space. In addition, $S(t)$ in Fig. 4 represents the interface separating the melt and the solid. Under such conditions, the temperature distribution may be expressed as $T_s = T_s(x,t)$ for the solid and $T_l = T_m$ for the liquid.

For linear heat flow, the one-dimensional heat conduction along the x-axis in the solid must satisfy:

$$\frac{\partial^2 T_s}{\partial x^2} = \frac{1}{\alpha_s}\frac{\partial T_s}{\partial t}, \quad 0 \leqslant x \leqslant S(t) \tag{1}$$

The initial and boundary conditions are:

$$T_s(x,0) = T_m, \quad \text{at } t = 0 \tag{2}$$

$$T_s(0,t) = T_0, \quad \text{at } x = 0 \tag{3}$$

$$T_s(x,t) = T_m, \quad \text{at } x = S(t) \tag{4}$$

$$k_s \frac{\partial T_s}{\partial x} = \rho_s L \frac{dS}{dt}, \quad \text{at } x = S(t) \tag{5}$$

Eqs. (1)–(5) are nonlinear due to the fact that the velocity of the solidification front is coupled with the temperature via Eq. (5). Because of the mathematical complexity associated with the "Stefan problems", only a few specialized cases have exact analytical solutions. The exact solution for the problem presented above is known as Neumann's solution [5].

According to Carslaw and Jaeger [5], to satisfy Eqs. (1)–(5), the normalized interface location ξ must have the form:

$$\xi = \frac{S(t)}{H} = 2\lambda\sqrt{\tau_s} \tag{6}$$

where τ_s is a non-dimensional time defined as $\tau_s = \alpha_s t/H^2$, and λ is the positive root of the following transcendental equation:

$$\lambda\sqrt{\pi}\exp(\lambda^2)erf(\lambda) = \mathrm{Ste} \tag{7}$$

Here, $erf(\lambda)$ is the Gaussian error function defined as $erf(\lambda) = (2/\sqrt{\pi})\int_0^{\lambda} e^{-V^2}dV$ and V is a dummy variable. For convenience, the Stefan number $Ste = c_p(T_m - T_0)/L$ is defined as the ratio of the sensible heat to the total latent heat in the solidification process. When $Ste \to 0$ (i.e., cooling temperature equal to the melting temperature), $\lambda = 0$, indicating that no solidification has taken place.

4. Treatment of pore inclusion

4.1. Assumptions

Of particular interest is how the location of the solidification front and full solidification time will be varied if pores are distributed in the melt. For example, solidification with gaseous pores within the melt is encountered during the fabrication of close-celled aluminum foams, which influences the quality of the cellular structure of the end products (and hence the mechanical, thermal, acoustic and other properties of the material) [15].

Solidification is a complex process involving many factors such as: (i) mathematical complexity of multidimensional transient heat transfer with moving boundary; (ii) dependence of physical properties on temperature, time, and space; and (iii) various physical and chemical reactions during the solidification process, either endothermic or exothermic, producing the additional heat generation. These apply for the solidification with and without the pore inclusion.

To simplify and better understand the solidification process in the fabrication of close-celled aluminum foams, the following assumptions are made: (i) no other heat generation except latent heat is present and (ii) all physical properties including (effective) thermal conductivity are invariant in temperature, time, and space. The latter appears to be reasonable for aluminum (alloy): the variation of its thermal conductivity with absolute temperature (ranging from the ambient temperature to the melting temperature) is less than 10% [22]. On the other hand, in the temperature range considered, the thermal conductivity of gaseous (i.e., H_2) pores varies dramatically up to 250% [22]. However, its value within the entire range of absolute temperature considered is not comparable to that of the continuous phase (the melt), low enough to neglect its contribution to the whole solidification process. Consequently, in the present analysis, the effects of the physical contents in the pores and their variations in temperature are ignored. This is equivalent to assume that the pores are in vacuum.

A new challenge arises with regard to the dealing of pores. This is due to the fact that metallic foams foaming with blowing agents are anisotropic as the isotropic distribution of gaseous pores in the continuous phase is hardly controllable and achievable. In addition, during the solidification, the pores move, grow, and may even disappear because of the instability of the melt. To simplify these, it is firstly assumed that the pores are relatively small in size in comparison with other physical dimensions of the metal foam, and randomly distributed in space so that the foam can be taken as a homogeneous medium with "stochastically" isotropic effective physical properties. Furthermore, close-celled aluminum foam is assumed to be heterogeneous, consisting of continuous dense materials and randomly distributed discrete gaseous pores. In the melt, the pores are assumed to be staying still during the whole process, with additional effects on pore surfaces neglected. In other words, the pores maintain the same size and location during the whole solidification process.

The thermal conductivity, heat capacity, and density of gas are considerably smaller in comparison with those of typical metals, e.g., aluminum (both in its liquid and solid state) and hence ignored. Since the density of the material was previously assumed to be constant for the liquid phase, natural convection in the melt is not considered. Typically, the pores in the melt have sufficiently small sizes for natural convection within the pore to be negligible [9]. In the present analysis, thermal radiation is also not considered. Consequently, the heat is transferred only by conduction in the solid and liquid.

4.2. Effective properties of close-celled foams

Thermal conductivity is a key parameter in any heat conduction problem. There exist several analytical models to obtain the effective thermal conductivity of a porous medium in steady state [23–26]. In the present study, the exact solution reported by Bauer [23] assuming that the porous medium is consisted of identifiable continuous and randomly distributed discrete phases is employed and combined with Neumann's solutions presented in Section 2 to solve the solidification problem for close-celled aluminum foams.

According to Bauer [23], the relationship between the effective thermal conductivity k_e of a porous medium and that of its compositions may be expressed as:

$$\frac{k_e - k_d}{k_s - k_d}\left(\frac{k_s}{k_e}\right)^{1-(2/3\beta)} = 1 - \varepsilon \tag{8}$$

where k_s and k_d are separately the thermal conductivities of continuous phase and discrete phase (pore), ε is porosity, and β is shape factor. The shape factor (β) given by the exact solution is equal to "1" for spherical pore (3-dimensional) and circular pore (2-dimemsional). Eq. (8) implies the dependence of the effective thermal conductivity on both the porosity and pore shape factor. For close-celled aluminum foams, only k_s will be considered since the conduction of heat via gaseous medium in the pores is negligible compared to that of the continuous phase. Consequently, Eq. (8) is reduced to,

$$k_e = k_s(1 - \varepsilon)^{3\beta/2} \tag{9}$$

According to Gibson and Ashby [9], the specific heat, latent heat, and fusion temperature of a porous material are equivalent to those of the dense parent material whilst its effective density ρ_e can be written as:

$$\rho_e = \rho_s(1 - \varepsilon) \tag{10}$$

where ρ_s is the density of the dense material. Substitution of Eqs. (9) and (10) into the definition of thermal diffusivity, $\alpha = k/\rho c_p$, leads to the following equation for the effective thermal diffusivity α_e:

$$\frac{\alpha_e}{\alpha_s} = f(\varepsilon, \beta) = (1 - \varepsilon)^{(3\beta/2-1)} \tag{11a}$$

which, for spherical and circular pores, simplifies to:

$$\frac{\alpha_e}{\alpha_s} = f(\varepsilon) = (1 - \varepsilon)^{1/2} \tag{11b}$$

4.3. Modified solution for solidification in close-celled foams

For porous media, the normalized interface location ξ of Eq. (6) needs be modified to account for the parameters associated with pore inclusion (e.g., porosity and pore shape), as:

$$\xi = 2\lambda\sqrt{\tau_e} \tag{12}$$

where τ_e is the non-dimensional time defined as $\tau_e = \alpha_e t/H^2$.

Substitution of Eq. (11) into (12) yields a modified solution for the location of solidification front in close-celled foams as:

$$\xi = 2\lambda\sqrt{f(\varepsilon, \beta)\cdot\tau} \tag{13}$$

where λ is determined by solving Eq. (7) and $f(\varepsilon, \beta)$ is defined by Eq. (11).

5. Numerical simulations

5.1. Physical and numerical models

Due to difficulties associated with the experimentation for solidification in close-celled foams, it is necessary to carry out numerical simulation to validate the analytical model introduced in this study. To this end, the finite difference method (FDM) embedded within a commercially available software Flow-3D™ is employed.

A physical model [15] and a numerically generated model for close-celled aluminum foam are shown in Fig. 5(a) and (b), respectively. The boundary conditions are fixed wall temperature at $x = 0$ and thermal insulation at $x = H$ (Fig. 5(b)). To ensure one-dimensional heat flow along the x-direction, boundaries in other directions are taken as symmetric. For simplicity, two-dimensional circular pores with varying sizes distributed randomly in space and having adiabatic pore boundaries (Fig. 5(b)) are used to simulate the (nearly) spherical pores of Fig. 5(a).

During the entire simulation, MATLAB™ is used to generate data for pores having different sizes and spatial locations, followed by solid model generation using a computer aided design (CAD) program. The solid model is then imported for the FDM simulation. It should be noted that during the generation of pores having random size, the upper and lower limits were set as 5.0 mm (for 5 pores per inch (PPI) foams) and 0.64 mm (for 40 PPI foams), respectively, to comply with the pore size variation of the actual close-celled foams in production. Here, the actual pore sizes and pore distance of closed-celled aluminum foams foaming with blowing agent were measured, based on images taken using a scanning electron microscopy (SEM).

5.2. Governing equations and boundary conditions

With the convection term and internal heat generation neglected, the governing equation for transient heat conduction with a moving boundary may be expressed as [27]:

$$\frac{\partial}{\partial t}(\rho \widetilde{H}) = \nabla \cdot (k \nabla T) \tag{14}$$

where ρ is density, and $\widetilde{H}$ is enthalpy equal to the sum of the sensible enthalpy $\tilde{h}$ and latent heat $\Delta\widetilde{H}$:

$$\widetilde{H} = \tilde{h} + \Delta\widetilde{H} = \left(\tilde{h}_{\mathrm{ref}} + \int_{T_{\mathrm{ref}}}^{T} c_p \mathrm{d}T\right) + (1 - f_s)L \tag{15}$$

Here, $\tilde{h}_{ref}$ and T_{ref} are the reference enthalpy and temperature, c_p is the specific heat at constant pressure, L is the total latent heat, and f_s is the solid fraction defined as:

$$f_s = \begin{cases} 0 & if \quad T > T_{liquidus} \\ \frac{T_{liquidus} - T}{T_{liquidus} - T_{solidus}} & if \quad T_{solidus} < T < T_{liquidus} \\ 1 & if \quad t < T_{solidus} \end{cases} \tag{16}$$

where T_{liquidus} and T_{solidus} are the liquidus and solidus temperatures, respectively.

In the FDM simulation, it is assumed that local thermal equilibrium is in force at the boundary between pores and dense material.

5.3. Consideration of pore shape

As described in references [23,26], both the pore shape as well as porosity affect the effective thermal conductivity of a porous medium. To examine the effect of the shape of individual pores on the effective thermal conductivity at a given porosity, the shape factor (β) in Eq. (9) was numerically obtained in steady state. Five different pore shapes (e.g., triangle, square, pentagon, hexagon, and circle) were considered in the present study. Fig. 6 shows the generated computational domains.

To numerically calculate β, unlike that illustrated in Fig. 5(b), a constant heat flux (q'') is imposed on the surface at $x = 0$ while the temperature at $x = H$ is fixed to be constant ($T_H = 300$ K). On the other hand, the temperature at $x = 0$, T_0, is allowed to vary according to the effective thermal conductivity (k_e) to be determined. Then, the effective thermal conductivity is calculated using Fourier's law, as:

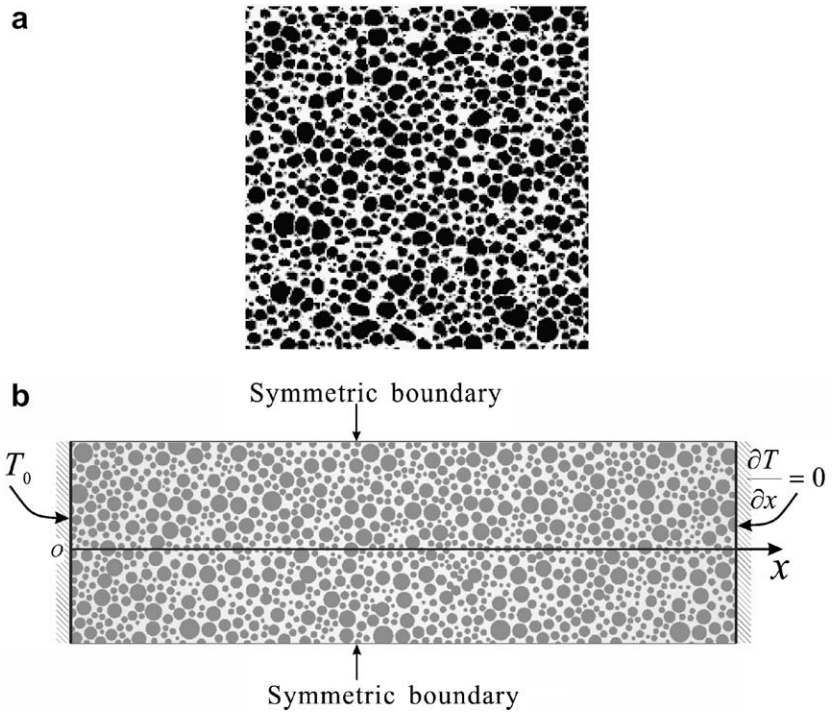

Fig. 5. Topology of close-celled foams: (a) image of close-celled aluminum foam with spherical pore and low porosity (~0.7) where black and white areas indicate gaseous medium and solid Al ligaments, respectively [15]; (b) computational model generated with boundary conditions.

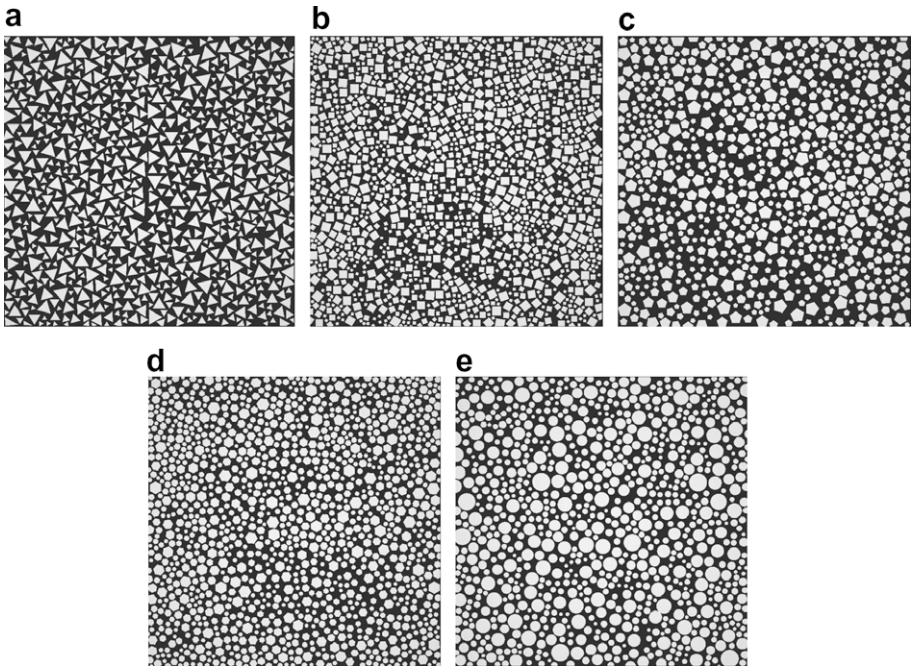

Fig. 6. Computational models of randomly distributed pores with different shapes: (a) triangle; (b) square; (c) pentagon; (d) hexagon; (e) circle.

$$q'' = -k_e \frac{T_0 - T_H}{H} \tag{17a}$$

where H is the thickness of the foam block coinciding with the direction of solidification (the x-axis). The calculated value of the effective thermal conductivity for each pore shape is then substituted into Eq. (9) to determine the shape factor.

6. Discussion of results

6.1. Solidification in close-celled foams with circular pores

Consider first a dense material without any pores ($\varepsilon = 0$), initially in liquid state at melting temperature T_m. At $t = 0$ (i.e., $\tau = 0$), the wall temperature at $x = 0$ is instantly dropped to a constant temperature T_0 ($<T_m$). As a result, solidification initiates from a region in the vicinity of the wall, $x = 0$. Fig. 7 shows how the location of the solid–liquid interface (i.e., solidification front) varies in time for a fixed Stefan number of 0.06. This value of Stefan number was chosen to facilitate the experimental validation of the dense material data [28]. The solid curve obtained from Neumann's solution Eq. (6) for $\varepsilon = 0$ (dense material) indicates a nonlinear and monotonic propagation of the solidification front, which agrees well with the present numerical simulation. However, both curves appear to deviate systematically from the experimental data reported by Xu and Naterer [28], although the overall trends are similar. This difference results from a time delay partly associated with the super-cooling when solidification is initiated, which is *not* considered in both the analytical model and numerical simulation. If a time delay say $\Delta\tau = 0.55$ is applied, both the analytical and numerical predictions collapse onto the experimental data points as shown by the dashed line in Fig. 7.

The nonlinear trend exhibiting in Fig. 7 is attributable to the fact that the solidification front moves slower as it moves away from the wall boundary $x = 0$. The conduction of heat in the solidified layer is governed by Fourier's law:

$$q'' = -k \frac{T_0 - T_m}{S(t)} \tag{17b}$$

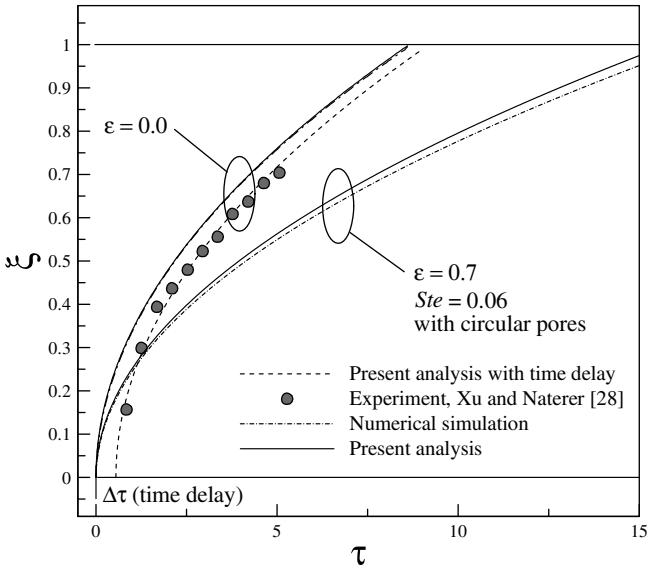

Fig. 7. Analytically and numerically predicted temporal evolution of solidification front (ξ) in the melt with randomly distributed circular pores for Ste = 0.06; test data for dense material are taken from Ref. [28].

For a given temperature difference (i.e., $T_0 - T_m$ = constant) and with the assumption of invariant thermal conductivity, the solidification front moves away from the wall boundary as time elapses. Therefore, the effective heat flux q'' traveling though the solidified layer is decreased in a nonlinear manner as $q'' \sim 1/S(t)$. This causes the deceleration of the solidification rate as the solid–liquid interface moves away from the wall boundary.

To examine the effects of pore inclusion in the melt on the overall solidification behavior of close-celled aluminum foam, a selected case of porosity $\varepsilon = 0.7$ (randomly distributed circular pores) is next considered. Results from the numerical simulations as well as analytical predictions Eq. (13) are presented in Fig. 7. The nonlinear and monotonic behavior of the solidification front

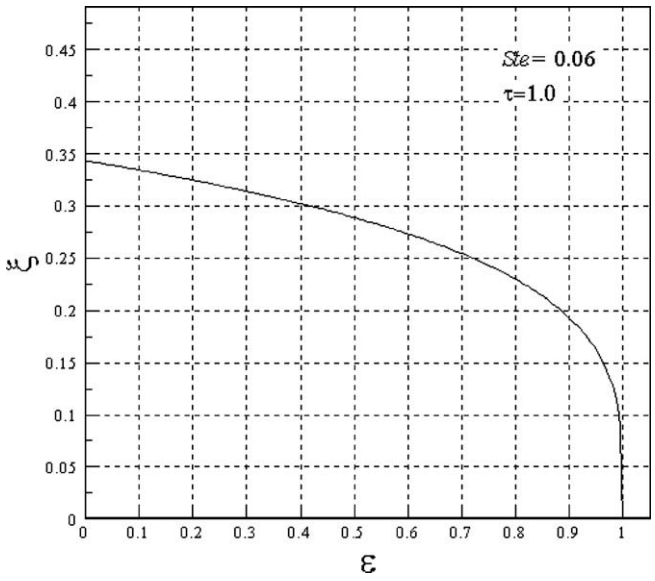

Fig. 8. Solidification front (ξ) plotted as a function of porosity for fixed Stefan number (Ste = 0.06) and time (τ = 1).

(same trend as the dense material) is clearly seen, although the presence of pores in the melt significantly delays the solidification. This retardation of the solidification can be explained by the reduction of effective thermal conductivity and diffusivity due to pore inclusion. With the presence of pores, the low thermal conductivity of gaseous medium acts to reduce the effective thermal conductivity of the solidified foam. For example, the effective thermal conductivity drops down to 16.4% of that of the dense material if $\varepsilon = 0.7$. Consequently, the solidification front only reaches about 72% of the total thickness of the material block by the time when the dense material is fully solidified. The results of Fig. 7 demonstrate that there is excellent agreement between analytical and numerical predictions, within a deviation approximately 5%. Given that the present analytical model is simple and expressed in closed-form, this agreement is remarkable.

As can be observed from Fig. 7, for a given cooling condition (Stefan number) and time (τ), the solidification for a lower porosity case progresses further towards the dense materials. To elaborate the effect of porosity on the location of the solidification front, a full range of porosity values is considered. As depicted in Fig. 8, the retardation of the solidification as a result of the increased porosity is gradual in the low porosity range (e.g., $\varepsilon < 0.7$) whereas the extent of the delay of the solidification drastically becomes pronounced for a further increase in porosity when $\varepsilon > 0.7$.

6.2. Effects of pore shape on solidification in close-celled foams

The presence of circular pores in the close-celled foam has been shown to strongly influence the solidification process. As above-mentioned, in most close-celled foams having relatively low porosities, the cross-sectional shape of the individual pores is likely to be circular; as the porosity is increased beyond 0.8, the pores tend to become non-circular [15]. It has been reported that the inclusion of non-circular pores leads to the variation of effective thermal conductivity although porosity is kept constant [26]. In such cases, the shape factor (β) needs to be determined in order to estimate its influence on the solidification process. Table 1 summarizes the numerically calculated shape factors. The exact solution [23] gives $\beta = 1$ for circular or spherical pores, identical to that obtained from the present numerical simulation. Polygonal pore geometries (e.g., triangle, square, pentagon, and hexagon) all have shape factors larger than unity, resulting from the lower effective thermal conductivity than that of the circular pore case for a given porosity (Table 1).

Adopting the calculated shape factors, we consider next the effects of randomly distributed pores having different pore shapes on the temporal evolution of the solidification front and full solidification time. Fig. 9(a) plots the temporal evolution of solidification for selected pore shapes, with the Stefan number fixed at 0.6 and the porosity at 0.7. As the pore shape changes from circular, hexagon, pentagon, and square to triangle, the solidification is increasingly delayed. This is attributed to the reduced effective thermal conductivity as the pore shape is varied, although the porosity is kept constant. For example, the solidification front of the close-celled foam with randomly distributed triangular pores has reached only 72% along the direction of the solidification by the time when the close-celled foam having circular pores is fully solidified.

The influence of pore inclusion with any pore shapes on the effective thermal conductivity as well as effective diffusivity of metal foams has been shown to be pronounced. Consequently, the overall solidification behavior of the porous material is greatly affected, as dictated by the key parameters – porosity and pore shape. How these two parameters change the full solidification time of the melt is considered below.

Fig. 9(b) displays the full solidification time predicted from the present analytical model as a function of porosity for five selected pore shapes. For circular pores, as the porosity is increased from the dense materials ($\varepsilon = 0$), the time required for the full solidification increases accordingly. The rate of increase, initially mild for low porosity materials, picks up as the porosity is approximately larger than 0.7. For example, the full solidification of porous materials takes 2 times (for $\varepsilon = 0.7$) and 3 times (for $\varepsilon = 0.9$) longer than that required for the dense materials to be fully solidified. For close-celled foams with porosities larger than 0.7, the time required for full solidification increases exponentially with increasing porosity as observed in Fig. 9(b). This implies that when dealing with low porosity materials, the thermal conductivity of dense materials dominates the full solidification time whilst porosity only plays a minor role. On the other hand, for high porosity materials ($\varepsilon > 0.7$), it is the porosity that plays the pivotal role in the overall solidification process. When non-circular pores are included in the melt, the overall patterns are similar whereas significant delay of the full solidification is clearly estimated. Especially with the triangular pores, it takes twice longer time for the melt to be fully solidified compared to the circular pores at $\varepsilon = 0.7$.

Table 1
Numerically calculated shape factors for different pore shapes for $\varepsilon = 0.5$ ($H = 0.1$ m and $q'' = 5.0 \times 10^4$ W/m^2 used for numerical simulation)

Pore shape	Number of sides	T_0[K]	T_L[K]	ΔT[K]	k_e/k_0	Shape factor β
Triangle	3	415.07	300.00	115.07	0.20	1.35
Quadrangle	4	389.84		89.84	0.25	1.14
Pentagon	5	387.93		87.93	0.26	1.12
Hexagon	6	385.03		85.03	0.27	1.10
Circle	Infinite	376.71		76.71	0.30	1.01

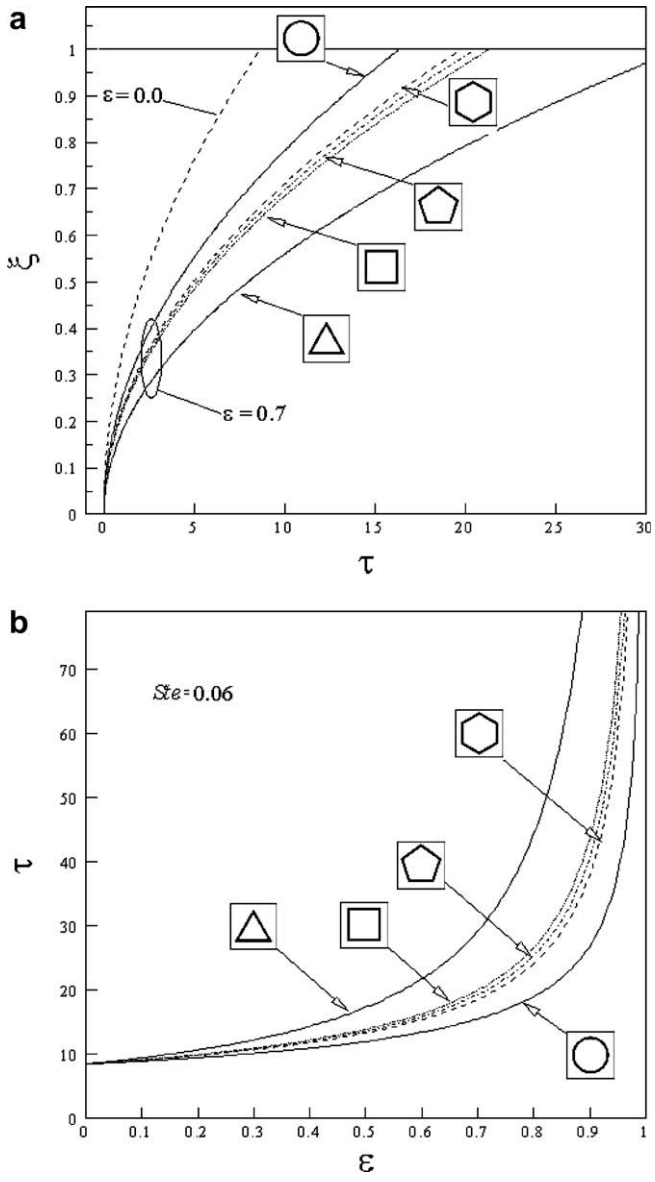

Fig. 9. Effects of pore shape on temporal evolution of solidification front (ξ) and full solidification time (τ) for Ste = 0.06: (a) solidification front; (b) full solidification time as a function of porosity (ε).

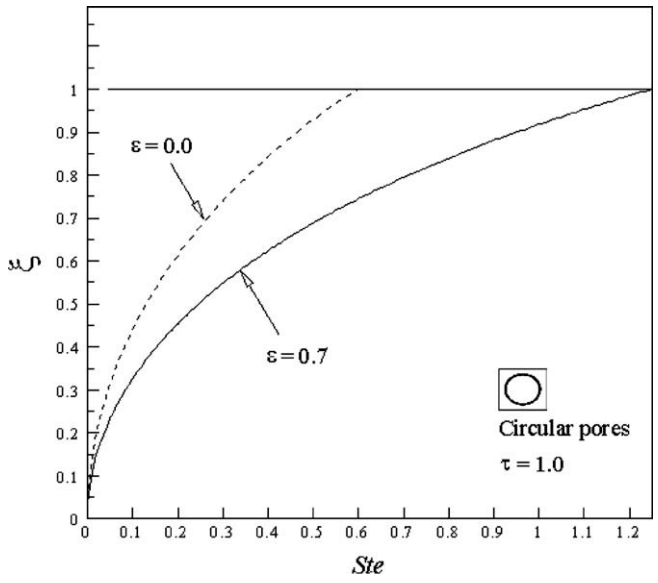

Fig. 10. Solidification front (ξ) plotted as a function of Stefan number for given porosities (ε = 0.0, 0.7) and time (τ = 1).

6.3. Effect of Stefan number on solidified melt thickness

The discussion hitherto on the overall solidification behaviors of close-celled aluminum foams also with various pore shapes has focused on fixed cooling conditions such as Ste = 0.06. It is obvious that when the wall boundary is exposed to a lower cooling temperature for a given material with known melting temperature T_m, the solidification front expects to move faster, thickening the solidified layer.

As the Stefan number $\mathrm{Ste} = c_p(T_m - T_0)/L$ varies in a way that either the temperature difference $(T_m - T_0)$ or the product of latent heat (L) and specific heat c_p is changed, the solidification process will behave in a different manner. The former is a controllable parameter before (and during) the solidification whereas the latter is fixed once the material is chosen. Considering a given material, e.g., aluminum, the only way to vary the Stefan number is to change the cooling temperature, T_0. An increase in Stefan number leads to the significant thickening of the solidified layer in a nonlinear-monotonic fashion as shown in Fig. 10 for the circular pore case. For the onset of solidification, even a small degree of temperature drop triggers the dramatic progress of solidification. Henceforth, the rate of increase is reduced as the Stefan number is further increased. Regardless of the porosity, this pattern remains unchanged whilst low porosity materials reach full solidification earlier than high porosity materials as previously discussed.

7. Conclusions

An analytical model to predict the location of solidification front and full solidification time under various cooling conditions for heterogeneous materials such as closed cell foams has been introduced. The classical solidification model (Neumann's solution for Stefan problems) and a preexisting analytical model of effective thermal conductivity for porous media are coupled to account for the influence of pore inclusion on solidification. The validity of model predictions is examined by comparing with full numerical simulations of the solidification of a dense material as well as model foam containing randomly distributed circular pores. Excellent agreement between analytical predictions and numerical results is achieved for both materials; for the dense materials, both the analytical and numerical predictions correlate well with experimental measurements.

The analytical model predicts that porosity plays a major role in the solidification of high porosity close-celled aluminum foams. For a fixed Stefan number, an increased porosity causes the delay of full solidification: about 2 times (ε = 0.7) and 3 times (ε = 0.9) longer for the circular pores in comparison with that of the dense material as a result of the reduced effective thermal conductivity and diffusivity. A further retardation of the solidification takes place if polygonal pores (e.g., triangle, square, pentagon, and hexagon pores) are posed in the melt for a given porosity. Furthermore, for a given porosity (and time), a decrease in cooling temperature (and hence an increase in Stefan number) leads to significant thickening of the solidified layer. The analytical model, simple and expressed in closed-form, can be used to guide the manufacturing of high quality close-celled metallic foams via the direct foaming route.

Acknowledgements

This work was supported by the National Basic Research Program of China (2006CB601202, 2006CB601203), The National Natural Science Foundation of China (10572111, 10632060), The National 111 Project of China (B06024) and The National High Technology Research and Development Program (2006AA03Z519).

References

[1] M.C. Flemings, Solidification Processing, McGraw-Hill Inc., 1974.
[2] J.C. Muehlbauer, J.E. Sunderland, Heat conduction with freezing or melting, Appl. Mech. Rev. 18 (12) (1965) 951–957.
[3] B. Zalba, J.M. Marin, L.F. Cabeza, H. Mehling, Review on thermal energy storage with phase change: materials, heat transfer analysis and applications, Appl. Therm. Eng. 23 (3) (2003) 251–283.
[4] J. Stefan, Uber die throrie der eisbildung, insbesondereuber die eisbildung in polarmaere, Ann. der Phys. und Chem. 42 (1891) 269–286.
[5] H.S. Carslaw, J.C. Jaeger, Conduction of Heat in Solids, Oxford University Press, Oxford, 1959.
[6] T.R. Goodman, The heat balance integral and its applications to problems involving change of phase, J. Heat Transf. 80 (3) (1958) 335–341.
[7] N.M.H. Lightfoot, The solidification of molten steel, Proc. Lond. Math. Soc. 31 (2) (1929) 97–116.
[8] R.I. Pedroso, G.A. Domoto, Inward spherical solidification-solution by the method of strained coordinates, Int. J. Heat Mass Transf. 16 (1973) 1037–1043.
[9] L.J. Gibson, M.F. Ashby, Cellular Solids: Structure and Properties, second ed., Cambridge University Press, 1997.
[10] J. Banhart, Manufacture, characterisation and application of cellular metals and metal foams, Prog. Mater. Sci. 46 (3) (2001) 559–632.
[11] T.J. Lu, F. Chen, D.P. He, Sound absorption of cellular metals with semi-open cells, J. Acoust. Soc. Am. 108 (4) (2000) 1697–1709.
[12] M.F. Ashby, T.J. Lu, Metal foams: a survey, Sci. Chin. Ser. B 47 (6) (2004) 512–520.
[13] M.F. Ashby, A.G. Evans, N.A. Fleck, L.J. Gibson, J.W. Hutchinson, H.N.G. Wadley, Metal Foams – A Design Guide, Butterworth-Heinemann, Oxford, 2000.
[14] J. Banhart, N.A. Fleck, A. Mortensen, Cellular Metals: Manufacture, Properties, Application, MIT Verlag, Berlin, 2003.
[15] Q.C. Zhang, T.J. Lu, S.Y. He, D.P. He, Control of pore morphology in closed-celled aluminum foams, J. Xi'an Jiaotong Univ. 41 (3) (2007) 255–270.
[16] V. Gergely, D.C. Curran, T.W. Clyne, The FOAMCARP process: foaming of aluminium MMCS by the chalk-aluminium re-action in precursors, Comp. Sci. Technol. 63 (16) (2003) 301–2310.
[17] Y. Zhou, D.P. He, J.Q. Jiang, New type of spherical pore Al alloy foam with low porosity and high strength, Sci. Chin. Ser. B 47 (5) (2004) 407–413.
[18] D.H. Yang, D.P. He, Thermal decomposition properties of titanium hydride and Al alloy foam with low porosity and small pore diameter, Chin. J. Nonferr. Met. 14 (12) (2004) 2021–2028.
[19] C.C. Yang, H. Nakae, The effects of viscosity and cooling conditions on the foamability of aluminum alloy, J. Mater. Proc. Technol. 141 (2) (2003) 202–206.
[20] H. Stanzick, M. Wichmann, J. Weise, L. Helfen, T. Baumbach, J. Banhart, Process control in aluminum foam production using real-time X-ray radioscopy, Adv. Eng. Mater. 4 (10) (2002) 814–823.
[21] M.J. Zheng, D.P. He, G. Dai, Additional force field in cooling process of cellular Al alloy, Sci. China Ser. B 45 (6) (2002) 598–607.
[22] F.P. Incropera, D.P. DeWitt, Fundamentals of Heat and Mass Transfer, third ed., John Wiley & Sons, New York, 1990.
[23] T.H. Bauer, A general analytical approach toward the thermal conductivity of porous media, Int. J. Heat Mass Transf. 36 (17) (1993) 4181–4191.
[24] H.W. Russell, Principles of heat flow in porous insulators, J. Am. Ceram. Soc. 18 (1) (1935) 1–5.
[25] A.L. Loeb, Thermal conductivity: VIII, a theory of thermal conductivity of porous materials, J. Am. Ceram. Soc. 37 (2) (1954) 96–99.
[26] J.F. Wang, J.K. Carson, M.F. North, D.J. Cleland, A new approach to modelling the effective thermal conductivity of heterogeneous materials, Int. J. Heat Mass Transf. 49 (17–18) (2006) 3075–3083.
[27] Flow Science, Inc., Flow-3D Manual, Santa Fe, New Mexico, USA. Available from: <www.flow3d.com>.
[28] R. Xu, G.F. Naterer, Deterministic physical influence control of interfacial motion in thermal processing of solidified materials, Exp. Therm. Fluid Sci. 29 (2) (2005) 227–238.